Journal of the American Ceramic Society

Voltage-Dependent Bulk Resistivity of SrTiO3:Mg Ceramics

Journal:	*Journal of the American Ceramic Society*
Manuscript ID:	JACERS-34147.R1
Manuscript Type:	Article
Date Submitted by the Author:	n/a
Complete List of Authors:	Gil-Escrig, Lidon; Jaume I University, Inorganic and Organic Chemistry Prades, Marta; Jaume I University, Inorganic and Organic Chemistry Beltran, Hector; Jaume I University, Inorganic and Organic Chemistry Cordoncillo, Eloisa; Jaume I University, Inorganic and Organic Chemistry Masó, Nahum; University of Sheffield, Materials Science and Engineering West, Anthony; University of Sheffield, Materials Science and Engineering
Keywords:	strontium titanate, sol-gel, electrical properties

Voltage-Dependent Bulk Resistivity of $SrTiO_3$:Mg Ceramics

Lidon Gil Escrig[1], Marta Prades[1], Héctor Beltrán[1], Eloisa Cordoncillo[1], Nahum Masó[2] and Anthony R. West[2,*]

[1] Departamento de Química Inorgánica y Orgánica, Universitat Jaume I, Avda. Sos Baynat s/n, 12071 Castellón, Spain.

[2] Department of Materials Science and Engineering, University of Sheffield, Mappin Street, S1 3JD Sheffield, United Kingdom.

[*] **Corresponding author.** E-mail address: a.r.west@sheffield.ac.uk; Telephone: +44 (0) 114 222 5501; Fax: +44 (0) 114 222 5943.

Abstract

Single phase ceramics of composition $Sr(Ti_{1-x}Mg_x)O_{3-x}$: $0 \leq x \leq 0.01$ were prepared by sol-gel synthesis and characterized by X-Ray diffraction, scanning electron microscopy, impedance spectroscopy and current-voltage measurements. The bulk and grain boundary conductivities increase on application of a small *dc* bias voltage in the range 3 to 200 Vcm^{-1} and at temperatures in the range 150 to 800 ºC. A qualitatively similar increase in conductivity occurs on increasing P_{O_2} in the surrounding atmosphere, which shows that conduction is *p*-type. The conductivity increase is reversible on removal of the *dc* bias or on reducing P_{O_2} and is not observed in undoped $SrTiO_3$. It is an intrinsic property of the bulk material, differs from the voltage-dependent effects observed with varistors and is attributed to changes in redox equilibria between oxygen species at the surface which cause changes in carrier concentration in the interior. A capacitive model of this low-field *dc* bias effect is presented and compared with a memristive model of high field resistance degradation.

Keywords: $SrTiO_3$; ceramics; sol-gel; electrical properties, memristors.

Introduction

$SrTiO_3$ (ST)-based oxides with high dielectric constant and low loss are of interest for applications in next-generation microelectronic and microwave devices. At room temperature, ST is cubic,

centrosymmetric and paraelectric. At low temperatures, its dielectric constant increases to ~10^4, where it is described as a quantum paraelectric [1]. ST undergoes a cubic to tetragonal phase transition at ~100 K [2]; this appears as a deviation from linearity of a Curie-Weiss plot and is responsible for a peak in tan δ vs temperature. Ferroelectric behaviour in ST can be induced by application of a high electric field [3] or uniaxial stress [4]. Haeni *et al.* [5] showed an increase of T_C with epitaxial strain, producing ferroelectricity at room temperature. The ferroelectric transition temperature is sensitive to chemical substitutions in the lattice, such as Ba or Ca into the Sr-site [6, 7]. Bianchi *et al.* [8] showed that $Sr_{1-x}Ca_xTiO_3$ becomes ferroelectric above x = 0.0018. Wei *et al.* [9] investigated the influence of A-site disorder in ST codoped with Ca and Ba and showed that the materials changed from quantum paraelectric to relaxor-like ferroelectric and eventually to classical ferroelectric.

The effect of Mg substitution in ST has been discussed [10, 11]; the solid solubility of Mg in ceramics prepared by the conventional mixed oxide route depends on the lattice site at which substitution occurs. Incorporation of Mg into the Ti site with oxygen vacancies for charge balance, $SrTi_{1-x}Mg_xO_{3-x}$, is more favourable and a higher solubility limit ($0 \leq x \leq 0.1$) was obtained compared with substitution at the Sr site ($0 \leq x \leq 0.01$ in $Sr_{1-x}Mg_xTiO_3$). Ti-site doping drives the system away from quantum paraelectric behaviour, decreasing both the maximum permittivity value and the dielectric loss at microwave frequencies.

We have reinvestigated the electrical properties of pure and Mg-doped ST, motivated by the recent discovery that the conductivity of other acceptor-doped perovskite ceramics, such as Mg-doped $BaTiO_3$ [12], increases on application of a small dc bias in the range 1-10V; on removal of the bias, the conductivity returns gradually to its original state. The increase in conductivity, which is p-type, was attributed to hole creation at underbonded lattice oxide ions in the vicinity of acceptor dopants; in chemical terminology, holes located on oxide ions rather than delocalised in a conduction band

are referred to as O^- ions. Given the current interest in p-type materials for transparent conductor applications, it was of interest to investigate the possibility of enhanced p-type conduction as well as bias-dependent conductivity in acceptor-doped $SrTiO_3$.

Experimental

Samples of $SrTi_{1-x}Mg_xO_{3-x}$, STM, ($0 \leq x \leq 0.01$), were prepared by sol-gel synthesis using $Sr(CH_3COO)_2$ (99%, Strem Chemicals), $Mg(CH_3COO)_2{\cdot}2H_2O$ (99.99% Sigma-Aldrich) and $Ti(C_3H_7O^i)_4$ (98%, with 2% iso-propanol, Strem Chemicals). Strontium acetate was dissolved in acetic acid and heated at 60 ºC with stirring; magnesium acetate was added to this solution followed by acacH (acacH = pentane-2,4-dione) and titanium isopropoxide; finally, methanol was added to give a clear solution which was left open in a desiccator to obtain a clear gel. Given the low Mg contents, sol-gel synthesis was preferred to solid state reaction to achieve better homogeneity.

The resulting gels were decomposed by heating at 5 ºC min^{-1} to 500 ºC, left at 500 ºC for 1 h and heated to 1000 ºC at 5 ºC min^{-1} with a final hold at 1000 ºC for 2 h. Pellets were prepared from crushed decomposed gel powder by uniaxial pressing, heated in air at 1400 ºC for 12 h and cooled slowly inside the furnace. Pellet densities were ~ 74 %.

The phase(s) present were analyzed by X-Ray Powder Diffraction, XRD, using a Bruker D4 Endeavor diffractometer, Cu$K\alpha$ radiation. The cubic lattice parameter was determined from XRD data by least-squares refinement for reflections in the range $15 < 2\theta < 70$º, using the software WinXPow version 1.06. Scanning electron micrographs (SEMs) of pellet surfaces and cross sections were taken on an SEM JEOL 7001F model equipped with a spectrometer for energy-dispersive analysis of X-rays (EDX). The samples for microstructure determination and microanalysis were deposited on an Al holder and coated with graphite.

For electrical property measurements, electrodes were fabricated on opposite pellet faces from Pt paste which was dried and decomposed by gradually heating to 900 ºC; for selected experiments, Au paste, which was decomposed at 800 ºC, was used. Samples with electrodes attached were placed into a conductivity jig and measured using a combination of Agilent 4294A, E4980A and Alpha-N Novocontrol impedance analysers over the frequency range 10 mHz to 13 MHz and temperature range –263 to 900 ºC. For subambient measurements, an Oxford Cryostat with Intelligent Controller (ITC5035) was used. Impedance data were corrected for pellet geometry and for the blank cell capacitance ('jig correction'). Current (I) vs voltage (V) measurements were carried out using a Keithley SourceMeter, Model 2410.

Results

Powders of $SrTi_{1-x}Mg_xO_{3-x}$, STM, ($0 \leq x \leq 0.01$) were single phase by XRD after firing at 1400 ºC. The patterns closely resembled those of cubic ST. According to the formula $SrTi_{1-x}Mg_xO_{3-x}$ with x = 0.01, the most likely crystal structure has 1% of the octahedral Ti sites occupied at random by Mg instead of Ti, together with creation of an equal number of oxygen vacancies. The general formula and the compositions studied were similar to those reported for Mg-doped $BaTiO_3$ (BT) [12]. Given the similar sizes of Ti and Mg, it is not surprising that little change was observed in the lattice parameters, varying from 3.9028(9) Å for x = 0 to 3.9032(8) Å for x = 0.01. Grain size in the range 2–10 μm was observed by SEM. Typical microstructure of x = 0.01, is shown in Fig 1. EDX results confirmed the presence of Sr, Ti and O, but Mg was not observed due to its small concentration. There was also no evidence of secondary phases or Mg segregation to the grain boundaries by backscattered electron analysis.

Typical results of impedance measurements, without application of a *dc* bias, on samples sintered at 1400 ºC for 12h, followed by slow cooling in air are shown in Fig 2 for composition x = 0.005. Two arcs are apparent in the impedance complex plane plots (a, b): a high-frequency arc of resistance R_1

and a large intermediate-frequency arc of resistance R_2. Therefore, resistances, R_1 and R_2 together dominated the total resistance (R_1+R_2).

Capacitance data for the different components were obtained by replotting the data as spectroscopic plots of capacitance C′ at different temperatures, as shown in Fig 2(c). These demonstrated a frequency-independent, but temperature-dependent plateau at high frequencies attributed to the bulk component, C_1. Its value, e.g. ~9×10^{-12} Fcm^{-1} at 25 ºC decreased with temperature. (Note: the capacitance units, Fcm^{-1} are corrected for sample geometry). A second plateau at lower frequency with value ~2×10^{-10} Fcm^{-1}, was attributed to a conventional grain boundary, C_2.

At the highest temperatures and lowest frequencies, C′ increased further to ~ 1 μF, Fig 2(d) inset (i), characteristic of a capacitance at the sample-electrode interface [13], but the value of Z" decreased to ~ 1 ohm, inset (ii), showing that the sample-electrode contact was essentially ohmic with a resistance of 1 ohm or less.

The impedance data, Fig 2, may be interpreted in terms of an equivalent circuit containing, ideally, three parallel RC elements connected in series; R_1C_1 and R_2C_2 represent the sample bulk and grain boundaries, respectively; R_3C_3 represents the sample-electrode interface, which is ohmic since $R_3 \leq$ 1 ohm. This implies that the sample is an electronic conductor entirely; any oxide ion conduction, if present, should be detected by a significant value of the charge transfer resistance, R_3, at the sample-electrode interface. Further, there was no evidence of any Warburg impedance for frequencies as low as 10 mHz which again, would be a characteristic of oxide ion conduction. Since $R_3 \leq$ 1 ohm, there was also no evidence of Schottky barriers at the sample-electrode interfaces; therefore, the results presented later on *dc* bias-dependence are not influenced by Schottky barriers. Detailed circuit analysis and fitting has not been carried out since the prime objective was to obtain

values of R_1 and R_2, which was possible by simple inspection. All datasets, including data for undoped ST, showed similar impedance response to that in Fig 2(a–c).

From impedance data such as shown in Fig 2(a, b), resistance values were extracted and are shown as conductivities σ_1 and σ_2 in Arrhenius format in Fig 2(e) with activation energy ~1.03 eV and ~1.33 eV, respectively. The σ_2 data do not represent accurately the grain boundary conductivities since they (and the capacitance values) are corrected only for the overall pellet geometry and not for the geometry of the grain boundary regions. Since C_2 is two orders of magnitude larger than C_1, the true σ_2 values should be correspondingly smaller by two orders of magnitude, assuming a brick layer model in which the magnitude of C is proportional to the thickness of the region responsible. There was little change in conductivity and activation energy with composition. Thus, all samples had resistive grain boundaries and conductive grains: typically, $R_2 \sim 100R_1$ and $C_2 \sim 100C_1$ and therefore, $\sigma_1 \sim 10^4\sigma_2$.

The effect of atmosphere during measurements without a *dc* bias is shown in Fig 2(f). The values of R_1 and R_2 are highest in N_2 and lowest in O_2; the conventional explanation for such atmosphere dependence is that conduction is predominantly *p*-type, equation (1), since holes are generated with increasing P_{O_2} :

$$\tfrac{1}{2}O_2 + V_O^{\bullet\bullet} \rightarrow O_O^x + 2h^{\bullet} \qquad (1)$$

In order to study the effect of voltage on the electrical properties, impedance measurements were carried out at the same time as a small *dc* bias, in the range 300 mV to 20 V, was applied across the sample corresponding to a voltage gradient of 3 to 200 Vcm^{-1}. Results showed a significant variation with voltage, time and temperature, as shown in Fig 3 (a, b).

R_1 decreased by 1 to 2 orders of magnitude with 10 V bias. Similar decreases (not shown) occurred for R_2. The rate of decrease was very temperature-dependent, as shown in Fig 4. The voltage-dependent changes were independent of the electrode material used (Pt or Au). No significant voltage-dependence of R_1 was observed in undoped ST, Fig 3(c) inset, although a decrease in R_2 by a factor of 2 to 3 was observed.

From the nature of the impedance plots, the resistances represent long range conduction through the sample. Thus, there was no evidence for any blocking capacitance in series with R_1 and R_2. The bias-dependent resistance is, therefore, not associated with localised dielectric relaxation such as dipole reorientation associated with, for instance, $Mg''/V_O^{\bullet\bullet}$ dipoles. On removal of the *dc* bias, R_1 and R_2 increased and the samples regained their original state, but the times taken were very temperature-dependent, Fig 4.

In Fig 3(d), both σ_1 and σ_2 for x = 0.005 increased with *dc* bias; σ_1 increased by one to two orders of magnitude to reach the steady state values shown, whereas the increase was less for σ_2. All Mg-doped samples showed a similar increase in σ_1; with undoped ST no effect of *dc* bias on σ_1 was seen, Fig 3(e), but a small increase in σ_2 occurred.

σ_1 data as a function of time are shown in Fig 4 for two temperatures after a bias voltage of 10V was applied, and after subsequent removal of the bias. With a bias, conductivities rose rapidly at first and then levelled off; the steady state values depended on the magnitude of the *dc* bias, as shown in Fig 5 at eg 420 ºC: σ_1 and σ_2 gradually increased and reached almost limiting values above 150 Vcm^{-1}. On removing the *dc* bias, conductivities decreased until reaching their initial value, Fig 4. The time required to recover the initial value was temperature dependent, eg ~2 days at 460 °C, but ~20 days at 380 ºC. On reversing the bias after a constant conductivity had been

obtained, the conductivity values initially decreased somewhat, but subsequently increased until the high conductivity state was again attained, Fig 6.

Since the time required to achieve a higher conductivity steady state on application of a *dc* bias, and also to return to the original, lower conductivity state on removal of the *dc* bias, was very temperature-dependent, it is clear that the rate limiting step(s) is (are) thermally activated. An approximate estimate of the activation energy was obtained by determining the time, τ, taken to reach a certain increment of the initial conductivity on application of the dc bias [14]. Results are shown in Fig 7 for the time taken to increase the conductivity by factors of 2.5, 3.3, 5.0 and 10.0 for five temperatures, although for the highest temperatures, >380ºC, the total increase in conductivity at the steady state was approximately one decade or less and an accurate τ value could not be obtained. The data shown are essentially linear; activation energies decreased from ~ 1.51 eV for the initial conductivity increase to 0.74 eV when averaged over a decade increase in conductivity. The activation energies are attributed tentatively to the processes involved in carrier creation and are of the same order of magnitude as that involved in electronic conduction, Fig 2 and 3, ~0.9 to 1.3 eV.

In order to investigate the possibility of *pn* junction creation, I-V characteristics were measured, as shown for x = 0.005 at 300 °C in Fig 8. An approximately linear ohmic response was observed with little evidence of non-linearity which could be characteristic of a *pn* junction, Fig 8 (inset).

The electrical homogeneity of samples, and any changes on application of a *dc* bias, was further investigated by analysis of impedance data in the M* formalism. In a plot of M" vs log ω, a peak corresponding to a parallel RC element is observed whose height is dependent on C^{-1}; its width, given by its FWHM (full width at half maximum), has a value of 1.14 decades for an ideal RC element. If the bulk response of a sample is non-Debye-like, or is the response of a distribution of

peaks associated with electrical heterogeneity, then an increase in FWHM is expected. The peak may be asymmetric for one of two possible reasons. First, M´´ peaks of homogeneous materials are characteristically broadened on the high frequency side, due to the inclusion of a constant phase element in the equivalent circuit that is usually needed to represent the non-ideal response [15]. Second, for heterogeneous materials, the M" peak may be broadened asymmetrically at either higher or lower frequencies, depending on whether the source of heterogeneity has higher or lower conductivity than the main part of the sample.

In Fig 9, an ideal Debye peak is shown together with M" peaks for x = 0.005 at 342 °C using data obtained without a *dc* bias and after a steady state had been reached with a *dc* bias. The experimental peaks are broadened, but not noticeably asymmetric. The peak associated with the *dc* bias is displaced to higher frequencies since the conductivity is higher (from $2\pi f_{max}RC = 1$ at the peak maximum, f_{max} is higher if R is smaller).

Experimental FWHM data obtained from M" peaks at different times after application and removal of a 10V bias are shown in Fig 10. FWHM increases initially, passes through a maximum, and then decreases to almost its original value. On removal of the bias, by contrast, the FWHM value stays constant, although the resistance increases. This shows that, on application of the *dc* bias, the sample becomes increasingly inhomogeneous electrically at short times before gradually returning to a more homogeneous state at longer times and gives important mechanistic information on the processes involved, as discussed later. On removal of the *dc* bias, the samples retain their electrical homogeneity but their resistance gradually increases.

The combined effect of changing P_{O_2} and application/removal of *dc* bias on the bulk conductivity of a sample of x=0.005 is shown in Fig 11. Measurements were carried out first in N_2, second in air and third in O_2, at 420 °C. For each atmosphere, the conductivity increased with *dc* bias; on

removal of the bias, the original conductivity value is regained after a sufficient period of time. In the absence of a bias, the conductivity also increased with P_{O_2}. These results taken together show conclusively that qualitatively similar changes in equilibria amongst surface-adsorbed oxygen species must be involved in the conductivity changes seen, both on application of a *dc* bias and on changing P_{O_2}

Discussion

The Mg-doped samples (x = 0.003, 0.005, 0.01) are *p*-type conductors and the grain boundary resistivity is several orders of magnitude higher than the grain resistivity. There was no evidence, from the impedance data, for significant levels of oxide ion conduction. On application of a *dc* bias, both grain and grain boundary conductivities increased with time before gradually levelling off; on removal of the bias, the conductivities decreased to their original values. The changes in grain conductivities were usually greater than those in grain boundary conductivities, apart from undoped ST which showed no sensitivity of grain conductivity to *dc* bias. The measured conductivities represent long-range electron transport rather than local dielectric relaxation.

In order to understand these results, we consider first a widely-accepted explanation for *dc* bias effects, primarily due to Waser *et al.* [14,16–23]. Dielectric ceramics containing oxygen vacancies, $V_O^{\bullet\bullet}$, incorporated by acceptor doping, show a slow increase in leakage current under *dc* field stress and with increasing temperature. This failure mechanism, known as resistance degradation, is believed to occur as a consequence of unmixing of the initially homogeneous concentration of oxygen vacancies [14,16–23]. We present our interpretation of this model, which we term a memristive model for reasons discussed later, in Fig 12(a).

On application of a *dc* bias, oxide ions migrate towards the anode (+vely charged). It is assumed that they do not discharge, as O_2 molecules, but instead fill oxygen vacancies near the anode

surface. To preserve electroneutrality, transition-metal acceptors (e.g. Fe, Ni) ionise, i.e. oxidise, creating holes and a *p*-type conduction region. The ionised electrons pass through the external circuit to the cathode where they are injected into the sample and, for titanate materials, enter the Ti 3d conduction band, i.e. Ti^{4+} is reduced to Ti^{3+}, leading to a *n*-type conduction region. These negatively-charged species balance the positive charge left by oxide ions that have migrated away from the cathode. Again, it is assumed that oxygen molecules from the atmosphere do not i) dissociate, ii) absorb, iii) ionise and iv) occupy the oxygen vacancies; therefore, the sample-cathode interface is also ionically blocking. Evidence for this mechanism comes from electrocoloration, especially when it is seen as an interface moving inward from the electrode-sample interface(s). However, Rodewald *et al.* [24] showed the incorporation of oxygen into Fe-doped $SrTiO_3$ single crystals during electrocoloration: oxygen exchange was observed in a crystal with Ag/Cr-electrodes using secondary ion mass spectrometry and microelectrode impedance measurements.

Between *n*- and *p*-type regions, a *pn* junction is formed [20]. When fully developed, the junction shows characteristic non-linear I-V response. No evidence of a *pn* junction was seen in our I/V data after degradation, Fig 8, although possibly, it was not sufficiently well developed to be seen in an I/V plot. In addition, on reversing the bias, conductivity values did not decrease with time to their initial value (bleaching process), Fig 6. In this sense, therefore, the results are not consistent with the model proposed to explain degradation [20].

The model shown in Fig 12(a) requires a certain degree of oxide ion conduction in the first instance which leads to mixed conduction involving three mobile species. A *p*-type region close to the anode and an *n*-type region close to the cathode are created; both electronic species are responsible for the observed increase in conductivity. This model is memristive since it requires a reverse bias to recover the initial state. In order for it to explain our results, it would require the annihilation of

mobile electronic species, and redistribution of oxide ion vacancies, to occur spontaneously as a self-discharge process on removal of the *dc* bias.

Such a mechanism has been used to explain resistance degradation in Al-doped ST ceramics and single crystals but no comment on the possible location of holes in the *p*-type anodic region has been made [20]. Since electronic conduction in such acceptor-doped materials is usually activated, it is relevant to consider where the holes are located. Although, in principle, valence band holes in oxides may form and be trapped at negatively-charged acceptors, the ionisation energy of Al^{3+} is extremely high and it is most unlikely that Al^{3+} could be ionised (this point is usually ignored in the literature). Similarly, other cations in the structure: Sr^{2+} and Ti^{4+} in Al-doped ST or Sr^{2+}, Mg^{2+} and Ti^{4+} in the present case, could not be the source of the holes. Unavoidable transition metal impurities can be discounted since no effect was seen here with undoped ST prepared from the same chemicals or with undoped BT and CT materials. We conclude, therefore, that the holes are located on oxygen as O^- ions. Examples of O^- species as trapped hole centres have been reported in Na- and Al-doped BT [25-27] and have been proposed to account for similar bias-dependent enhanced conductivity in acceptor-doped BT and CT [12, 28–31].

We propose that the source of holes is underbonded oxygens in the vicinity of acceptor dopants which ionise readily, leaving O^- ions; these holes are the principal carriers responsible for the enhanced conductivity. The acceptors that substitute for Ti^{4+} in the octahedral sites are accompanied by adjacent oxygen vacancies to preserve local electroneutrality. However, the remaining oxide ions surrounding the acceptors are significantly underbonded since one of their cationic neighbours, the acceptor, is divalent instead of tetravalent.

This explanation finds support in the well-known observation that the O^{2-} ion is unstable in the gas phase, where it would spontaneously ionise to give the O^- ion. It is stabilised in crystal lattices only

by the additional lattice energy associated with divalent rather than monovalent anions. Oxide ions adjacent to an acceptor do not have the same degree of stabilisation as an oxide ion in a defect-free lattice and are suggested to ionise readily in a relatively small potential gradient. Oxide ions at surfaces and interfaces provide another possible source of holes, independent of acceptors; this may be the origin of bias-dependent, grain boundary conductivity observed in undoped ST, Fig 3(e).

The next question concerns the ionised electrons and why they do not give rise to *n*-type conduction; they must be trapped somewhere. It appears that the ionised electrons are trapped at surface states, and indeed, trapping of these electrons provides the driving force for ionisation. The conductivity, which is *p*-type, is therefore enhanced, reversibly, on application of a small *dc* bias because of an increase in hole concentration.

Recently, we observed the opposite effect to that reported here in two *n*-type materials: Mn-doped $BaTiO_3$ and lightly-reduced TiO_2. In both cases the conductivity decreased reversibly on application of a small *dc* bias [32]. The explanation was relatively straightforward: *n*-type carriers were removed from the sample, trapped at the surface by a similar displacement in redox equilibria between various surface oxygen species and consequently, the conductivity decreased.

With both *p*-type and *n*-type materials, the conductivity changes on application of a *dc* bias are similar to those observed on changing the oxygen partial pressure in the atmosphere, which is a standard test for whether materials are *p*-type or *n*-type. To explain the P_{O_2} dependence, oxygen molecules absorb on the ceramic surface with increasing P_{O_2} and ionise by trapping electrons from the sample interior according to the idealised equation (1). If the conductivity increases with increasing P_{O_2}, conduction is *p*-type since withdrawal of electrons leads to an increase in hole concentration, and conversely for *n*-type conduction.

We propose that application of a small *dc* bias also favours ionisation of absorbed O_2 molecules on the sample surface and withdrawal of electrons from the sample interior. In reality, equation (1) is an oversimplification since various neutral and ionised oxygen species are likely to be present at the sample surface. Equilibria between various species can be envisaged starting from the adsorption of O_2 molecules until their full ionisation and dissociation to give lattice oxide ions that occupy pre-existing oxygen vacancies, either at the surface or in the interior, as shown:

Increasing $P_{O_2} \rightarrow$

$$O_2(g) \underset{\text{step 1}}{\longleftrightarrow} O_2(ads) \underset{\text{step 2}}{\overset{e^-}{\longleftrightarrow}} O_2^- \underset{\text{step 3}}{\overset{e^-}{\longleftrightarrow}} O_2^{2-} \underset{\text{step 4}}{\longleftrightarrow} 2O^- \underset{\text{step 5}}{\overset{2e^-}{\longleftrightarrow}} 2O^{2-}(surface) \longleftrightarrow 2O^{2-}(bulk) \qquad (2)$$

Equilibria between the different species may be displaced in either direction depending on conditions. Explanation of the decreased conductivity in *n*-type materials with a *dc* bias is straightforward, since one or more of the equilibria in (2) is displaced to the right hand side, leading to the removal of mobile electrons from the sample interior. For *p*-type acceptor-doped ST, similar changes to the surface equilibria occur, but removal of electrons from the sample interior leads to ionisation of under-bonded O^{2-} ions, an increase in hole concentration and an increase in conductivity.

Several stages are involved in the equilibria shown in (2). At present, we cannot comment on the relative likelihood of these various possibilities during either changes to P_{O_2} or on application of a *dc* bias, but note that, in the case of acceptor-doped BT, *dc* bias effects were observed even when the sample was evacuated. This indicates that pre-existing traps must be present, spontaneously, at any time, on the surface of such oxide ceramics. In surface science, it is well-established that partially-reduced oxygen species are present at sample surfaces [33-36] but their existence in electroceramics and their effect on the electrical properties, has received little attention so far.

Based on the results reported here and those in earlier publications [12,28-32], the model illustrated in Fig 12(b) is proposed. In response to an applied voltage, changes in equilibria between various oxygen species at the sample surface occur (equation 2); specifically, the concentration of reduced species at the anode increases. The electrons that cause the reduction come from the interior, initially from regions close to the surface, and arise from underbonded oxide ions in the vicinity of acceptor dopants, which ionise. Consequently, a capacitive charging process is envisaged leading to a negatively-charged surface and a positively-charged, *p*-type, accumulation layer associated with O^- ions.

With time, the accumulation layer thickens, inside the ceramic, as progressively more underbonded oxide ions are ionised. In favourable cases, the accumulation layer may extend across the entire sample, and reach the cathode-sample interface. As the number of O^- ions, i.e. holes, increases, the overall conductivity increases; the rate of increase slows down, Fig 4, since, at increasing distance from the anode, the potential drop experienced by the underbonded oxide ions decreases and there is less driving force for ionisation. The number of holes created also depends on the magnitude of the bias, as shown by the increase in conductivity with increasing bias, Fig 5.

The accumulation layer has higher conductivity than the original sample, leading to electrical inhomogeneity. We see evidence for the development of electrical inhomogeneity on application of a *dc* bias in Fig 10. The FWHM of M" spectra increases with time for short times, but decreases at longer times. Therefore, a distribution in resistances develops, in particular by the introduction of components with lower resistance but at longer times, the more resistive components gradually disappear and the samples become increasingly homogeneous again. Similar effects were observed in acceptor-doped BT [12]. The process described is capacitive rather than memristive and is reversed simply by removing the *dc* bias without the need to apply a reverse bias. There is a close

parallel between the effects of applying a *dc* bias and increasing P_{O_2}: the same mechanisms are responsible in both cases.

Models for voltage-dependent resistance

We now summarise the main features of the memristive and capacitive models which could be considered as models for the phenomena reported here.

(i) Memristive model, Fig 12(a).

- Oxygen vacancies electromigrate towards the cathode where they pile up; oxygen molecules from the atmosphere do not dissociate, ionise and occupy the oxygen vacancies, since they are blocked by the electrode. In order to balance the positive charge of the increased concentration of oxygen vacancies, electrons enter the sample at the cathode leading to an *n*-type region.
- Oxide ions migrate towards the anode where they do not discharge, as O_2 molecules, since they are blocked by the electrode. In order to balance charge, transition metal acceptors (e.g. Fe, Ni) oxidise, creating holes, leading to a *p*-type region.
- Between *n*- and *p*-type regions, a *pn* junction is formed. When fully developed, it shows characteristic non-linear I-V response.
- A certain degree of oxide ion conduction is required in the first instance which leads to mixed conduction involving oxygen vacancies, holes and electrons. Both electrons and holes are responsible for the observed increase in conductivity.
- The process is electrochemical in origin and requires a reverse bias to recover the original state. For this reason, the model is described as memristive.
- There is no gas-solid exchange of oxygen at either electrode. Electrocoloration results indicate that this may be the case with blocking electrodes although oxygen exchange can occur with non-blocking electrodes [24]. If significant oxygen exchange does occur, at both

electrodes, the system effectively becomes an oxygen pump, whose transport number is given by the contributions of ionic and electronic species to the overall conductivity.

(ii) Capacitive model, Fig 12(b).

- The effect of a small dc bias is to increase the concentration of reduced oxygen species at the anode as a consequence of changes in equilibria between various oxygen species, equation 2, at the sample surface; the changes are similar to those that result from increasing the partial pressure of oxygen surrounding the sample.
- The electrons that cause the reduction arise from underbonded oxide ions in the sample interior, particularly those in the vicinity of acceptors, which ionise.
- An accumulation layer of holes forms and thickens progressively. In favourable cases, the accumulation layer extends across the entire sample and reaches the cathode-sample interface.
- Oxide ion conduction is not an essential prerequisite. Holes are the main species responsible for the observed increase in conductivity.
- The process is capacitive, through creation of a negatively-charged surface and a positively-charged, interior accumulation layer. It is reversed spontaneously by removing the bias although the charged state could be preserved by rapid cool to lower temperatures.
- The capacitive model is able to account for the low field results reported here. The memristive model is unsatisfactory in several ways, but may be applicable with different materials and/or in different circumstances.
- The time-dependent increase in conductivity at low voltages is similar to that found in *dc* electrical degradation at high fields > 1000 Vcm^{-1} [22,23]. However, degradation is often observed at lower temperature than used here and higher voltages/longer times may be required to see similar phenomena. Given the differences in experimental conditions, it is possible that degradation and the effects reported here have a common origin.

Conclusions

Mg-doped ST ceramics with formula $Sr(Ti_{1-x}Mg_x)O_{3-x}$: $0 \leq x \leq 0.01$ have been prepared by sol-gel synthesis. Their conductivity increases on application of a small *dc* bias at temperatures in the range 150 to 800 ºC. This low field effect, not observed in undoped ST, is attributed to the defect structure of Mg-doped ST which contains substitutional Mg^{2+} ions adjacent to underbonded oxide ions, which ionise readily to give a more conductive excited state dominated by hole conduction; the ionised electrons are trapped at the surface by partially ionised oxygen species. The conductivity increase is reversible on removal of the bias, since electrons trapped at the surface are released and recombine with the holes.

A capacitive model is proposed to account for the observations and compared with features of a memristive model. The capacitance is determined by charge separation between reduced oxygen species at the anode interface and a positive accumulation layer in the sample interior associated with O^- ions. The capacitance is, however leaky because the conductivity of the sample, which is in parallel with the capacitance, increases under the action of a dc bias. The capacitive model does not require the segregation of oxygen vacancies. There is no evidence for oxide ion conduction in the impedance data, although oxygen vacancy migration has been reported in other perovskite systems [22, 24, 37].

All samples showed a grain boundary resistance which was larger than the bulk resistance. Whilst grain boundary resistances were also sensitive to dc bias, a larger effect was seen with the sample bulk resistances. We conclude that the bias-dependent effects are primarily associated with the sample bulk and not with interfacial effects, either at grain-grain contacts or at sample-electrode interfaces. Thus, the possibility of Schottky barrier formation and its bias-dependence is excluded from influencing the observed conductivity changes.

Undoped ST ceramics showed no effect of dc bias on the bulk resistance but did show an effect on the grain boundary resistance, similar to that of doped samples. We speculate that underbonded oxide ions at sample surfaces and interfaces may have been responsible.

These results demonstrate how the bulk properties of a ceramic, Mg-doped ST, are controlled by electron transfer reactions at the sample surface which depend on both P_{O_2} and a small dc bias. The effects observed may be enhanced by the high internal surface area of the rather porous ceramics; further work on dense ceramics or single crystals to quantify the effect of surface area would be beneficial.

Acknowledgements

We thank the EPSRC (NM, ARW) and "Universitat Jaume I"- project No. P1 1B2013-65 (MP, HB, EC) for financial support. MP thanks Universidad Jaume I for a fellowship (CONT/2011/08).

References

[1] K.A. Muller and H. Burkard, "$SrTiO_3$: an intrinsic quantum paraelectric below 4 K," Phys. Rev. B, **19**, 3593–3602 (1979).

[2] F.W. Lytle, "X-ray diffractometry of low temperature phase transformations in Strontium Titanate," J. Appl. Phys., **35**, 2212-2215 (1964).

[3] J. Hemberger, P. Lunkenheimer, R. Viana, R. Bohmer and A. Loidl, "Electric field-dependent dielectric constant and nonlinear susceptibility in $SrTiO_3$," Phys. Rev. B, **52**, 13159–13162 (1995).

[4] H. Uwe and T. Sakudo, "Stress-induced ferroelectricity and soft phonon modes in $SrTiO_3$," Phys. Rev. B, **13**, 271–286 (1976).

[5] J.H. Haeni, P. Irvin, W. Chang, R. Uecker, P. Reiche, Y.L. Li, S. Choudhary and W. Tian, "Room-temperature ferroelectricity in strained $SrTiO_3$," Nature, **430**, 758–761 (2004).

[6] J.G. Bednorz and K.A. Müller, "$Sr_{1-x}Ca_xTiO_3$: an XY quantum ferroelectric with transition to randomness," Phys. Rev. Lett., **52**, 2289–2292 (1984).

[7]. V.V. Lemanov, E.P. Smirnova, P.P. Syrnikov and E.A. Tarakanov, "Phase transitions and glass-like behavior in $Sr_{1-x}Ba_xTiO_3$," Phys. Rev. B, **54**, 3151–3157 (1996).

[8] U. Bianchi, K.A. Müller and J.G. Bednorz, "Raman scattering of ferroelectric $Sr_{1-x}Ca_xTiO_3$, x = 0.007," J. Phys. Condns. Matter, **6**, 1229–1238 (1994).

[9] T. Wei, C. Zhu, K.F. Wang, H.L. Cai, J.S. Zhu and J-M Liu, "Influence of A-site codoping on ferroelectricity of quantum paraelectric $SrTiO_3$," J. Appl. Phys., **103**, 124104 (2008).

[10] A. Tkach, P.M. Vilarinho and A Kholkin, "Effect of Mg doping on the structural and dielectric properties of Strontium Titanate ceramics, "Appl. Phys. A, **79**, 2013–2020 (2004).

[11] A. Tkach, P.M. Vilarinho, A. Kholkin, A. Pshkin, P. Samoukhina, J. Pokorny, S. Veljko and J. Peltzelt, "Lattice dynamics and dielectric response of Mg-doped $SrTiO_3$ ceramics in a wide frequency range, "J. Appl. Phys., **97**, 044104 (2005).

[12] M. Prades, N. Masó, H. Beltrán, E. Cordoncillo and A.R. West, "Field enhanced bulk conductivity of $BaTiO_3$:Mg ceramics, "J. Mater. Chem., **20**, 5335–5344 (2010).

[13] J.T.S. Irvine, D.C. Sinclair and A.R West, "Electroceramics: characterization by impedance spectroscopy, "Adv. Mater., **2**, 132–138 (1990).

[14] R. Waser, T. Baiatu and K.H. Härdtl, "Degradation of dielectric ceramics, "Mat. Sci. Eng A, **109**, 171–182 (1989).

[15] D.P. Almond and A.R. West, "Impedance and modulus spectroscopy in "real" dispersive conductors," Solid State Ionics, **11**, 57-64 (1983).

[16] J. Blanc and D.L. Staebler, "Electrocoloration in $SrTiO_3$: Vacancy drift and oxidation-reduction of transition metals," Phys. Rev. B, **4**, 3548–3557 (1971).

[17] S.K. Mohapatra and S. Wagner, "Electrochromism in nickel-doped strontium titanate," J. Appl. Phys., **50**, 5001–5006 (1979).

[18] W.A. Schulze, L.E. Cross and W.R. Buessem, "Degradation of $BaTiO_3$ ceramic under high ac electric field," J. Am. Ceram. Soc., **63**, 83–87 (1980).

[19] R. Waser, "Electrochemical boundary conditions for resistance degradation of doped alkaline-earth titanates," J. Am. Ceram. Soc., **72**, 2234–2240 (1989).

[20] R. Waser, T. Baiatu and K.H. Härdtl, "dc electrical degradation of perovskite-type titanates: I, Ceramics," J. Am. Ceram. Soc., **73**, 1645–1653 (1990); II, "Single crystals," J. Am. Ceram. Soc., **73**, 1654–1662 (1990); III, "A model of the mechanism," J. Am. Ceram. Soc., **73**, 1666–1673 (1990).

[21] S. Rodewald, J. Fleig and J. Maier, "Resistance degradation of iron-doped strontium titanate investigated by spatially resolved conductivity measurements," J. Am. Ceram. Soc., **83**, 1969–1976 (2000).

[22] S.H. Yoon, C.A. Randall and K.H. Hur, "Effect of acceptor (Mg) concentration on the resistance degradation behavior in acceptor (Mg)-doped $BaTiO_3$ bulk ceramics: I. Impedance Analysis," J. Am. Ceram. Soc., **92**, 1758–1765 (2009); II. "Thermally Stimulated Depolarization Current Analysis," J. Am. Ceram. Soc., **92**, 1766–1772 (2009).

[23] S.H. Yoon, C.A. Randall and K.H. Hur, "Influence of grain size on impedance spectra and resistance degradation behavior in acceptor (Mg)-doped $BaTiO_3$ Ceramics," J. Am. Ceram. Soc., **92**, 2944–2952 (2009).

[24] S. Rodewald, N. Sakai, K. Yamaji, H. Yokokawa, J. Fleig and J. Maier, "The effect of the oxygen exchange at electrodes on the high voltage electrocoloration of Fe-doped $SrTiO_3$ single crystals: a combined SIMS and microelectrode impedance study," J. Electroceram., **7**, 95-105 (2001).

[25] E. Possenriede, P. Jacobs and O.F. Schirmer, "Paramagnetic defects in $BaTiO_3$ and their role in light-induced charge transport: I. ESR studies," J. Phys.: Condens. Matter, **4,** 47194742 (1992).

[26] T. Varnhorst, O.F. Schirmer, H. Kröse and R. Scharfschwerdt, "O^- holes associated with alkali acceptors in $BaTiO_3$," Phys. Rev. B, **53**, 116–125 (1996).

[27] O.F. Schirmer, "O− bound small polarons in oxide materials," J. Phys.: Condens. Matter, **18**, R667–R704 (2006).

[28] H. Beltrán, M. Prades, N. Masó, E. Cordoncillo and A.R. West, "Voltage-dependent low-field bulk resistivity of $BaTiO_3$:Zn ceramics," J. Am. Ceram. Soc., **93**, 500–505 (2010).

[29] N. Masó, M. Prades, H. Beltrán, E. Cordoncillo, D.C. Sinclair and A.R. West, "Field enhanced bulk conductivity of acceptor doped $BaTi_{1-x}Ca_xO_{3-x}$ ceramics," App. Phys. Lett., **97**, 062907 (2010).

[30] H. Beltrán, M. Prades, N. Masó, E. Cordoncillo and A.R. West, "Enhanced conductivity and non-linear voltage-current characteristics of non-stoichiometric $BaTiO_3$ ceramics," J. Am. Ceram. Soc., **94**, 2951–2962 (2011).

[31] Q-L Zhang, N. Masó, Y. Liu, H. Yang and A.R. West, "Voltage-dependent low-field resistivity of $CaTiO_3$:Zn ceramics," J. Mater. Chem., **21**, 12894–12900 (2011).

[32] M. Prades, H. Beltrán, E. Cordoncillo, P.J. Alonso, N. Masó and A.R. West, "Non-ohmic phenomena in Mn-doped $BaTiO_3$," Phys. Stat. Sol. A, **209**, 2267–2272 (2012); Y. Liu and A.R. West, "Voltage-dependent resistance of undoped rutile, TiO_2, ceramics," Appl. Phys. Lett., **103**, 263508 (2013).

[33] H. Ibach, "Physics of surface and interfaces." New York: Springer; (2006).

[34] A. Zangwill, "Physics at surface." New York: Cambridge University Press; (1996).

[35] H.H. Kung, "Transition metal oxides: surface chemistry and catalysis."Netherlands: Elsevier; (1991).

[36] P.T. Moseley and J.O.W. Norris, "Techniques and mechanisms in gas sensing." USA: Adam Hilger; (1991)

[37] P. Ren, N. Maso, Y. Liu, L. Ma, H. Fan and A.R. West, "Mixed oxide ion and proton conduction and p-type semiconduction in $BaTi_{0.98}Ca_{0.02}O_{2.98}$ ceramics," J. Mater Chem. C, **1**, 2426 (2013).

Figure Captions

Fig 1. SEM of the pellet surface (a) and cross section (b) of $SrTi_{0.99}Mg_{0.01}O_{2.99}$ sintered at 1400 ºC.

Fig 2. For $SrTi_{0.995}Mg_{0.005}O_{2.995}$, impedance complex plane plot at (a) 321 ºC and (b) 480 °C; (c) capacitance spectroscopic plot at different measuring temperatures; (d) impedance complex plane plot at 800 ºC with low frequency data shown as insets for (i) C' and (ii) Z"; (e) Arrhenius plots for σ_1 and σ_2; (f) Impedance complex plane plot at 634 ºC with different measuring atmospheres for $SrTi_{0.997}Mg_{0.003}O_{2.997}$.

Fig 3. Impedance complex plane plots for a) $SrTi_{0.995}Mg_{0.005}O_{2.995}$ at 280 ºC, b) $SrTi_{0.99}Mg_{0.01}O_{2.99}$ at 288 ºC and c) $SrTiO_3$ at 629 ºC before and after a voltage of 10 V was applied; d,e) Arrhenius plots for σ_1 and σ_2 before and after a voltage of 10 V was applied for $SrTi_{0.995}Mg_{0.005}O_{2.995}$ and $SrTiO_3$.

Fig 4. Bulk conductivity as a function of time measured with 10V (126 Vcm^{-1}) *dc* bias and after removal of the *dc* bias at (a) 460 ºC and (b) 380 ºC for $SrTi_{0.995}Mg_{0.005}O_{2.995}$.

Fig 5. Bulk (closed symbols) and grain boundary (open symbols) steady state conductivities as a function of *dc* bias at 420 ºC for $SrTi_{0.995}Mg_{0.005}O_{2.995}$.

Fig 6. Bulk conductivity as a function of time measured with 10V (126 Vcm^{-1}) *dc* bias and after reversing the *dc* bias at 400 ºC for $SrTi_{0.995}Mg_{0.005}O_{2.995}$.

Fig 7. Log τ vs 1/T for conductivity increase with 10V (126 Vcm^{-1}) for $SrTi_{0.995}Mg_{0.005}O_{2.995}$.

Fig 8. Current (I) vs voltage (V) at 300 °C for $SrTi_{0.995}Mg_{0.005}O_{2.995}$ and voltages over the range -30V to +30V. Inset: schematic non-linear response characteristic of a *pn* junction.

Fig 9. M" spectroscopic plots for an ideal Debye peak and for two typical M" peaks for x = 0.005, obtained without a *dc* bias (0 V) and after application of 18 V for 1440 min.

Fig 10. FWHM data for an M" peak showing the effect of application and after removal of a *dc* bias (**18V**) using data on composition x = 0.005 obtained at 342ºC.

Fig 11. Bulk conductivity at 420 ºC for $SrTi_{0.995}Mg_{0.005}O_{2.995}$ after applying and removing a *dc* bias of 10V [126 Vcm^{-1}] at different times in N_2, air and O_2.

Fig 12. (a) Memristive model and (b) Capacitive model for voltage-dependent resistance.

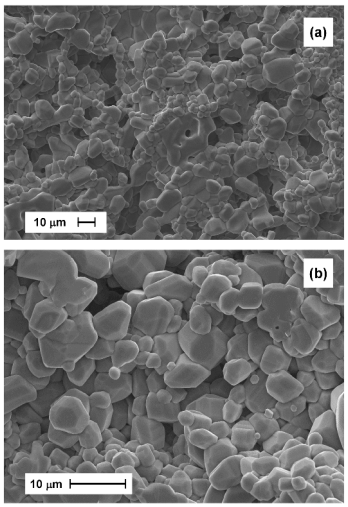

SEM of the pellet surface (a) and cross section (b) of SrTi0.99Mg0.01O2.99 sintered at 1400 ºC.
339x1187mm (150 x 150 DPI)

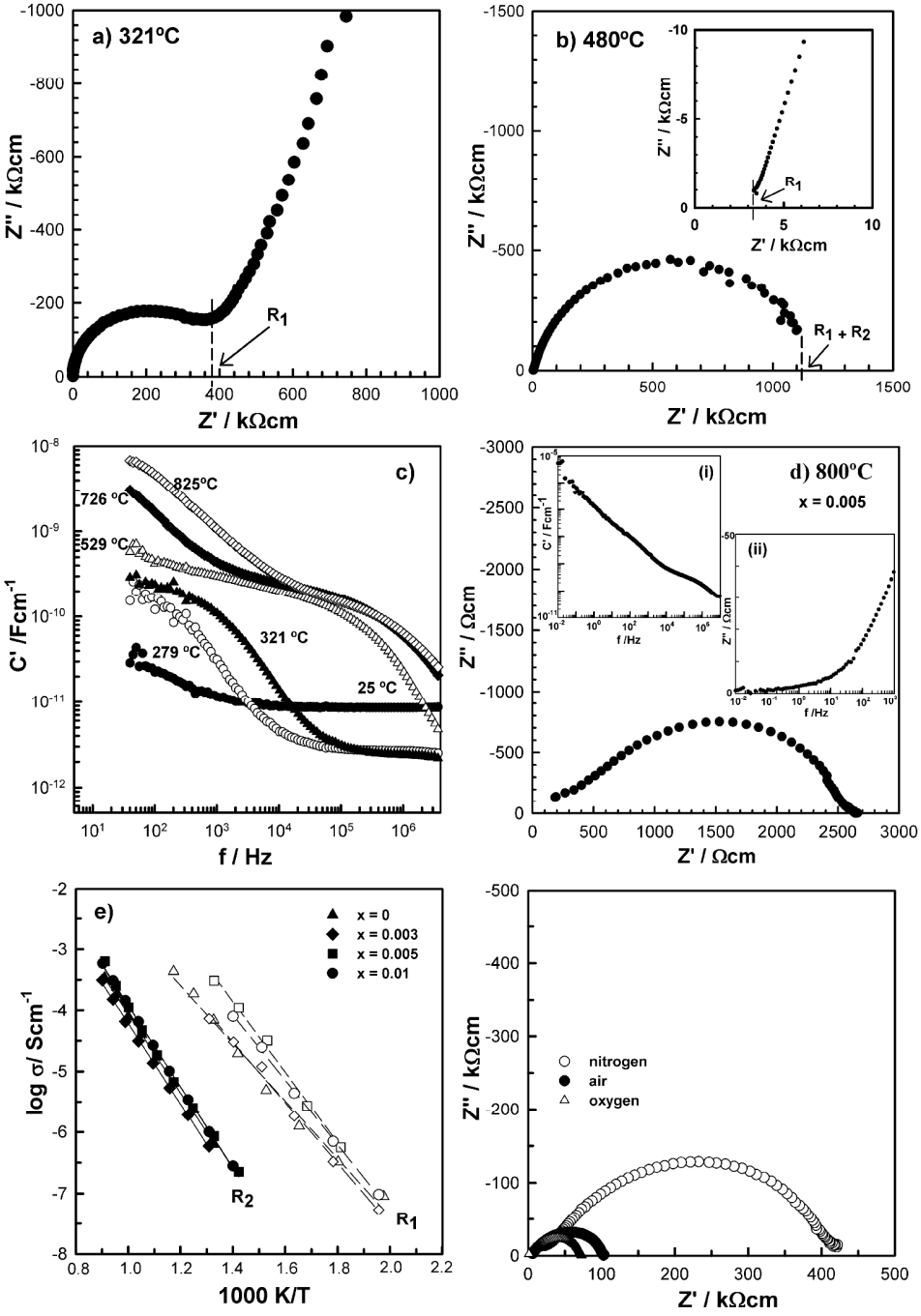

Fig 2. For $SrTi_{0.995}Mg_{0.005}O_{2.995}$, impedance complex plane plot at (a) 321 ºC and (b) 480 °C; (c) capacitance spectroscopic plot at different measuring temperatures; (d) impedance complex plane plot at 800 ºC with low frequency data shown as insets for (i) C' and (ii) Z"; (e) Arrhenius plots for σ_1 and σ_2; (f) Impedance complex plane plot at 634 ºC with different measuring atmospheres for $SrTi_{0.997}Mg_{0.003}O_{2.997}$.

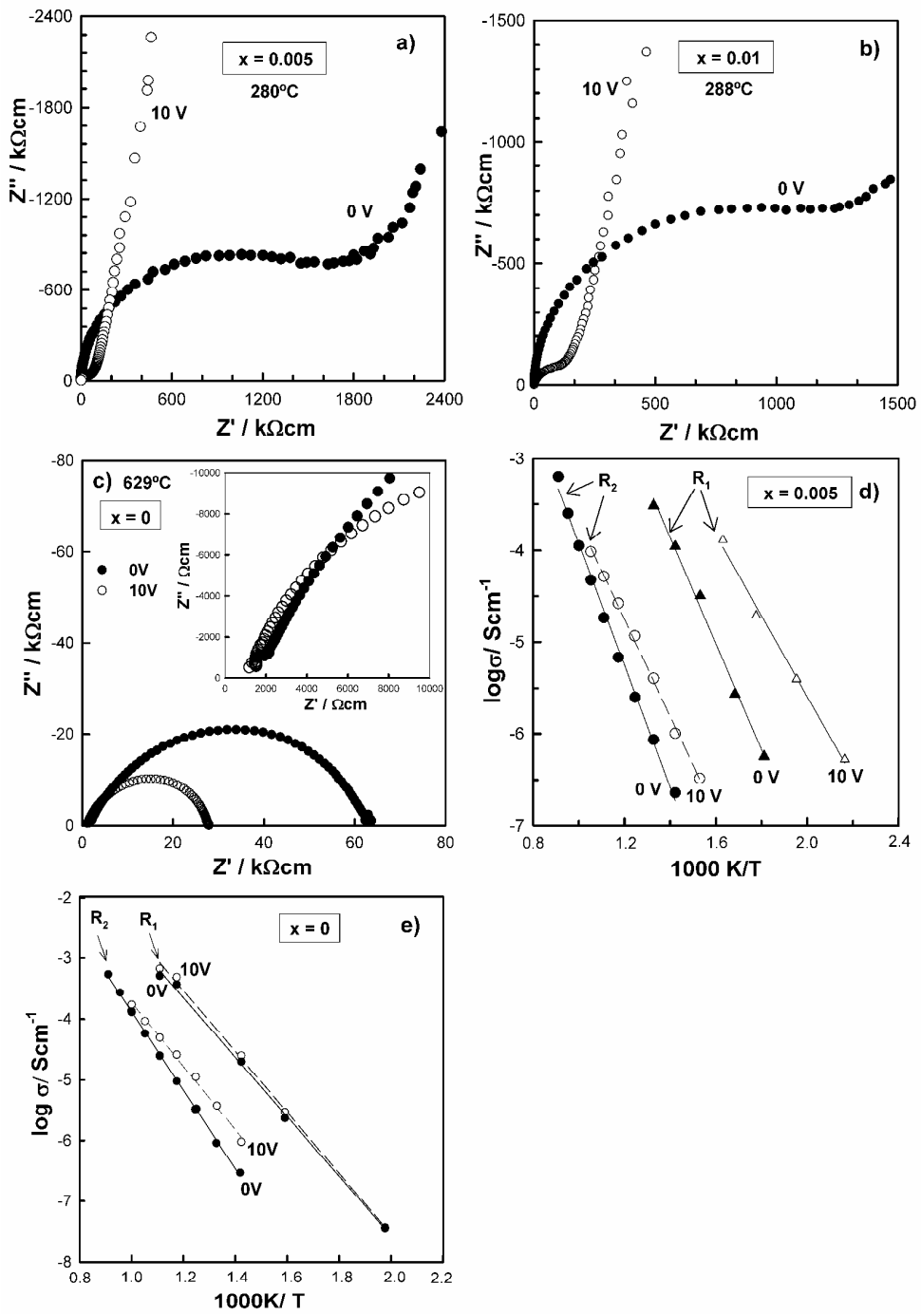

Fig 3. Impedance complex plane plots for a) $SrTi_{0.995}Mg_{0.005}O_{2.995}$ at 280 ºC, b) $SrTi_{0.99}Mg_{0.01}O_{2.99}$ at 288 ºC and c) $SrTiO_3$ at 629 ºC before and after a voltage of 10 V was applied; d,e) Arrhenius plots for σ_1 and σ_2 before and after a voltage of 10 V was applied for $SrTi_{0.995}Mg_{0.005}O_{2.995}$ and $SrTiO_3$.

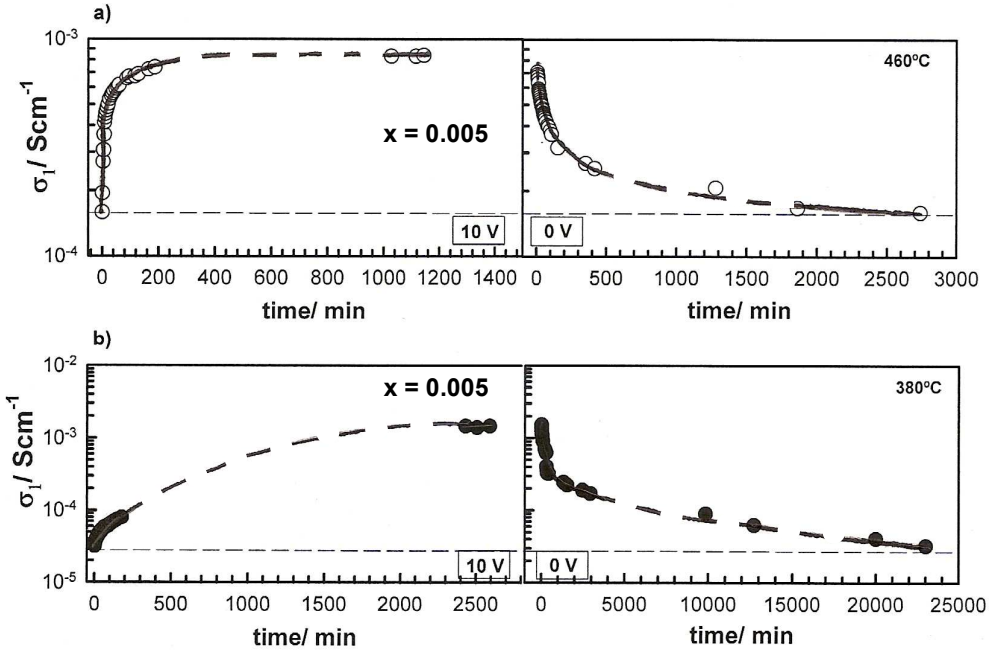

Fig 4. Bulk conductivity as a function of time measured with 10V (126 Vcm^{-1}) *dc* bias and after removal of the *dc* bias at (a) 460 ºC and (b) 380 ºC for $SrTi_{0.995}Mg_{0.005}O_{2.995}$.

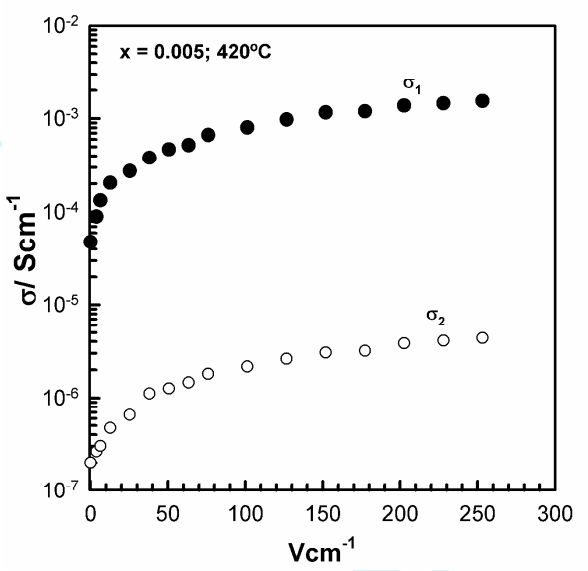

Fig 5. Bulk (closed symbols) and grain boundary (open symbols) steady state conductivities as a function of *dc* bias at 420 ºC for $SrTi_{0.995}Mg_{0.005}O_{2.995}$.

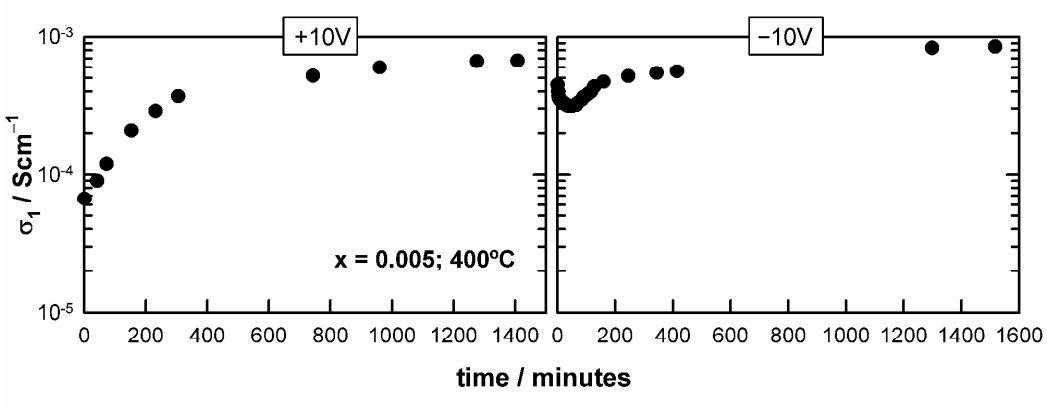

Fig 6. Bulk conductivity as a function of time measured with 10V (126 Vcm^{-1}) *dc* bias and after reversing the *dc* bias at 400 ºC for $SrTi_{0.995}Mg_{0.005}O_{2.995}$.

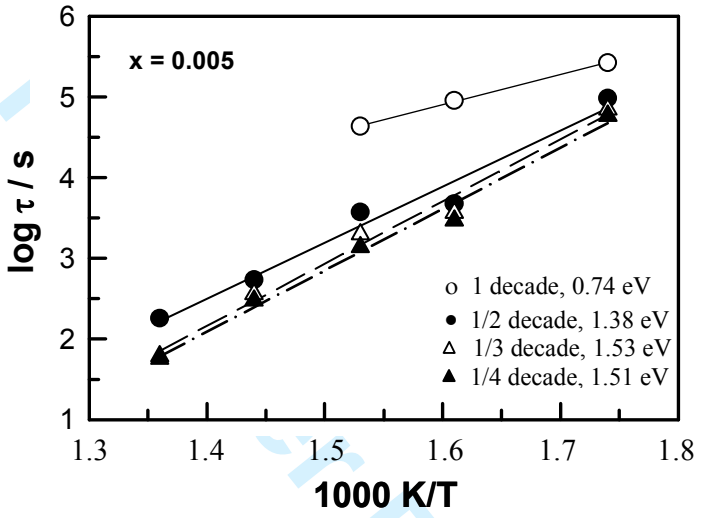

Fig 7. Log τ vs 1/T for conductivity increase with 10V (126 Vcm^{-1}) for $SrTi_{0.995}Mg_{0.005}O_{2.995}$.

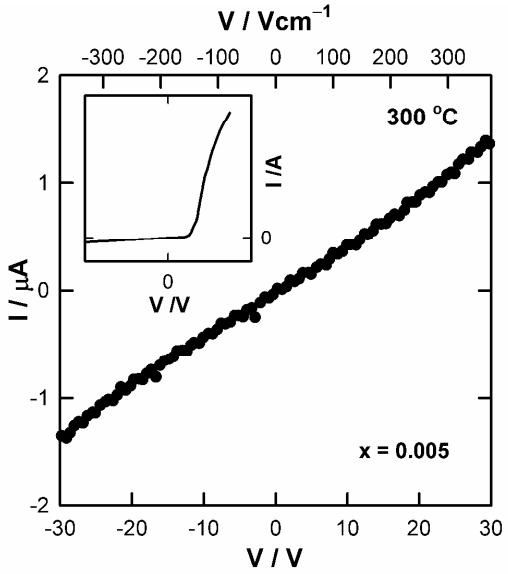

Fig 8. Current (I) vs voltage (V) at 300 °C for $SrTi_{0.995}Mg_{0.005}O_{2.995}$ and voltages over the range -30V to +30V. Inset: schematic non-linear response characteristic of a *pn* junction.

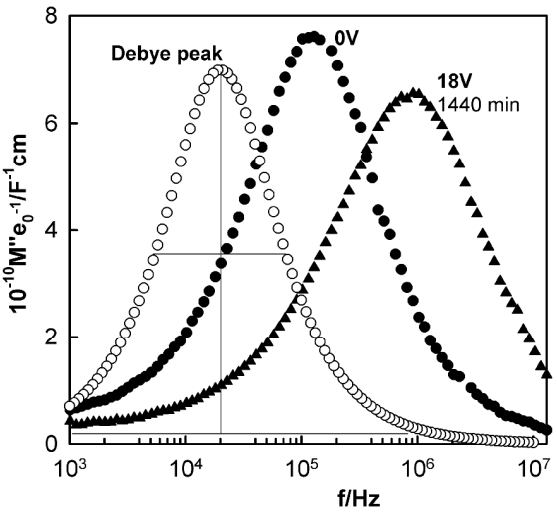

Fig 9. M" spectroscopic plots for an ideal Debye peak and for two typical M" peaks for x = 0.005, obtained without a *dc* bias (0 V) and after application of 18 V for 1440 min.

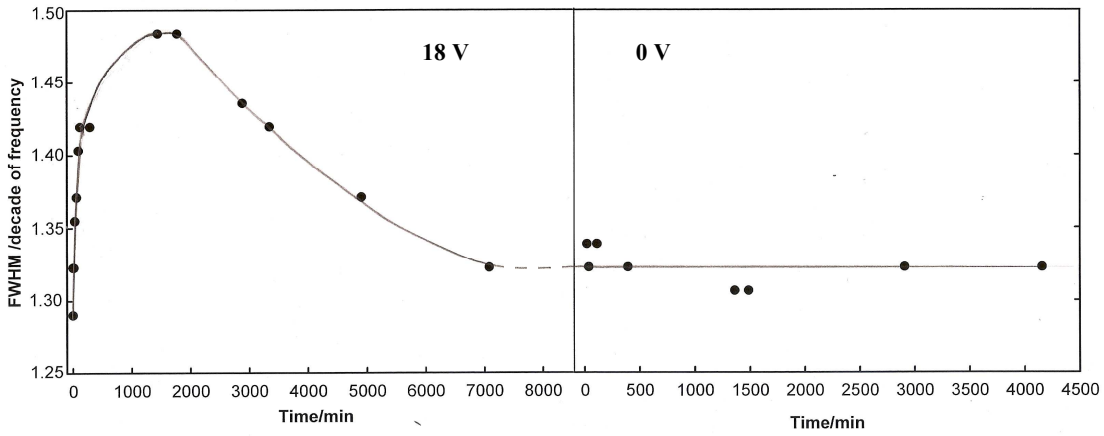

Fig 10. FWHM data for an M" peak showing the effect of application and after removal of a *dc* bias (**18V**) using data on composition x = 0.005 obtained at 342ºC.

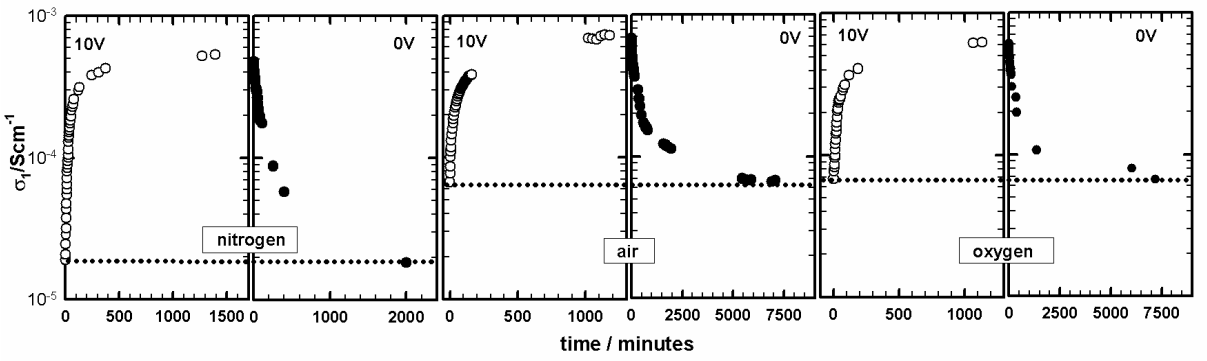

Fig 11. Bulk conductivity at 420 ºC for $SrTi_{0.995}Mg_{0.005}O_{2.995}$ after applying and removing a *dc* bias of 10V [126 Vcm^{-1}] at different times in N_2, air and O_2.

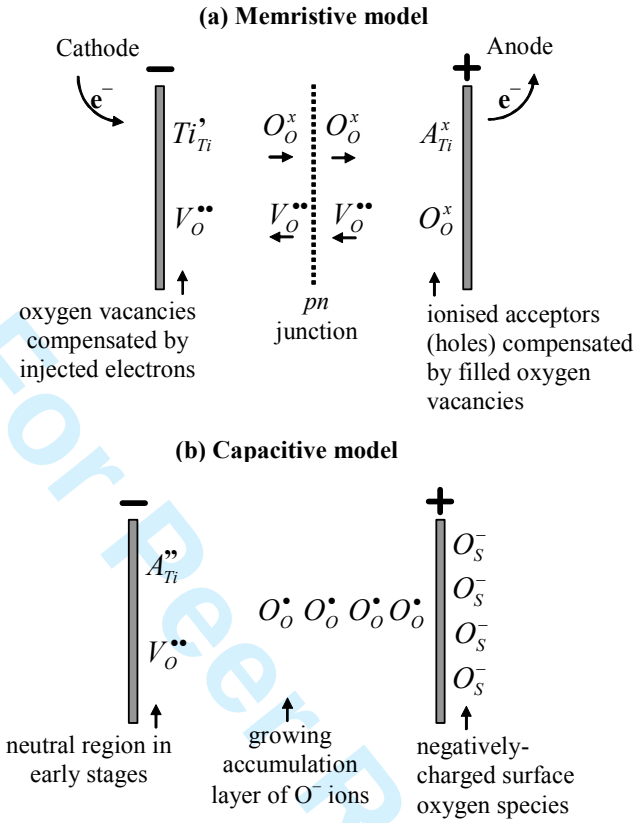

Fig 12. (a) Memristive model and (b) Capacitive model for voltage-dependent resistance.